QUARKS: Brazilian Electronic Journal of Physics, Chemistry and Material Science
journal homepage: https://periodicos.ufjf.br/index.php/quarks
e-ISSN: 2674-9688

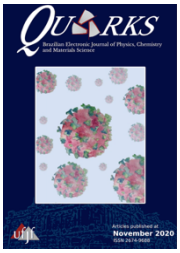

An Impurity Effect for the Rates of the Interparticle Coulombic Decay

Vladislav A. Guskov[a,b,c], Fabian Langkabel[a,d], Matthias Berg[a], Annika Bande[a*]

[a] *Helmholtz-Zentrum Berlin für Materialien und Energie GmbH, Hahn-Meitner-Platz 1, 10409 Berlin, Germany*
[b] *Moscow Institute of Physics and Technology (MIPT), Institutskiy Pereulok 9, Dolgoprudny 141701, Moscow Region, Russia*
[c] *Section de Mathématiques, Université de Genève, CH-1211, Geneva 4, Switzerland*
[d] *Institut für Chemie, Humboldt-Universität zu Berlin, Unter den Linden 6, 10099 Berlin, Germany*

Article history: Received: August 2020; Revised: September 2020; Accepted: October 2020. Available online: November 2020.
https://doi.org/10.34019/2674-9688.2020.v3.31928

Abstract

The interparticle Coulombic decay is a synchronized decay and ionization phenomenon occurring on two separated and only Coulomb interaction coupled electron binding sites. This publication explores how drastically small environmental changes in between the two sites, basically impurities, can alter the ionization properties and process rate, although the involved electronic transitions remain unaltered. A comparison among the present electron dynamics calculations for the example of different types of quantum dots, accommodating a one- or a two-dimensional continuum for the outgoing electron, and the well-investigated atomic and molecular cases with three-dimensional continuum, reveals that the impurity effect is most pronounced the stronger that electron is confined. This necessarily leads to challenges and opportunities in a quantum dot experiment to prove the interparticle Coulombic decay.

Keywords: Interparticle Coulombic decay, quantum dot, electron dynamics, impurity.

1. Introduction

The interparticle Coulombic decay (ICD [1]) is the decay process of an electronic Feshbach resonance state [2, 3, 4]. As such it relies on a higher-order reorganization of the electronic structure, as one electron is emitted only upon relaxation of another one [5, 6]. A peculiarity of ICD is that the two involved electrons are spatially much separated being located on two remote subsystems that are either only atoms [7, 8], molecules [1], quantum dots [9, 10], thin films [11] or the same species in combination with fullerenes [12, 13], proteins [14], graphene [15], etc. In one of the subsystems a local excited state relaxes in a single-electron transition and by Coulomb coupling makes its energy available for ionization of the other subsystem. The process requires only a few femtoseconds in clusters of atoms with interatomic separations of a few Ångströms. In nanostructures with separations in the range of 100 nm among the two subsystems, ICD terminates within the order of 100 ps. This is a result of the rate equation [16, 17] that reflects dipole-dipole coupling for the two electronic transitions leading to the ICD rate $\Gamma \propto R^{-6}$, which is depending on the separations R at negative sixth power. Its speed further depends on the explicit electronic situation and in particular the amount of transferred energy E in that $\Gamma \propto E^{-4}$.

The rate equation was shown to nicely hold in atomic pairs. In systems with a confined continuum, for which the studied cases were quantum dot pairs, the rates generally follow the mentioned trends on average, but to render at the same time rates that

*Corresponding author. E-mail: annika.bande@helmholtz-berlin.de

scatter around the expected values [9]. This scattering originates in the effective Coulomb double barrier that the electron in the originally excited quantum dot imposes on the outgoing ICD electron allowing sometimes for tunneling and sometimes not [9]. Other comparisons among the rate equation and electron dynamics after a change of the electronic structure through geometric parameter variation revealed further factors that make the rate unpredictable simply through a set of coupled dipole transitions [18, 19].

In superexchange ICD [20, 21, 22] the electronic structure is altered by introducing a neighbor that, however, plays an active role. This was originally an atom, which catalysis the ICD process by supporting virtual anionic states in conjunction with the ICD participators. Those couple to the final state wavefunction and, thus mediate the superexchange pathway. In this way the ICD rate experiences a significant enhancement by a factor of five, when bringing the extra atom from a theoretically infinite distance closer into the center of the bond [20]. A similar investigation was done for ICD in QD pairs, in which superexchange ICD was found to play a crucial role in rate enhancement when being placed in between or next to the two QDs [23].

We modify the electronic structure of the confined system in a different way without changing the two quantum dots themselves and without adding necessarily a further electron binding site. Instead, we propose to add a passive barrier or a potential well to the system, which is eventually not even electron binding. According to the analytical predictions for ICD in well-separated subsystems [16, 17], ICD should not at all depend on such passive additional neighbors. Nonetheless, we seek for a small environmental change, maybe only an impurity, which anyway leads to a large effect for the rate. To distinguish such impurity effect from superexchange ICD, we are going to explore the effect both for large distances among the three centers and for the central potential being only very shallow. Superexchange ICD instead can only be operative at short distances among the two original atoms or QDs [20, 21, 22, 23].

Experimentally, both impurity scenarios, binding and barrier, are accessible in the QD embedding material through doping, crystal structure or material alternation, or electric gating along the carrier material. If such alternations are small, they can be considered as defects or impurities in the hosting material, e.g. the wire [24]. Such planar defects were found to affect both the carrier mobility (by a factor below one order of magnitude). They would either cause a Coulomb blockade as is the barrier we are introducing here. Otherwise, they would introduce an electron confinement, which is reflected by our binding potential.

Furthermore, we will consider the degree of confinement, as we are aware that rates are more sensitive to energy-level changes when the continuum electron is more confined [9, 25]. For realistic quantum dots it is going to be illustrative how strong an additional potential can affect the processes in different classes of QDs. Hence, QDs in a wire [26, 27, 28, 29, 30], gated two-dimensional electron gas (2DEG) [30], and self-assembled QDs are considered here [31, 32, 33].

In the course of this publication the modeling of the QDs and the theoretical description are explained in the Theory and Computational Details, sections 2 and 3. The results are first presented for the nanowire QDs in section 4. The computationally more expensive, and hence scarcer results for the self-assembled QDs are then discussed in comparison to those. In the discussion of the section 5, an asset on the impact of the results is unfolded leading to the Conclusions, section 6, of the work.

2. Theory

The investigation on impurity effects on ICD in QDs is done by solving the electronic time-dependent Schrödinger equation for two electrons in a triplet state using the multiconfiguration time-dependent Hartree method (MCTDH) [34, 35] in the Heidelberg implementation [36, 37].

The full Hamiltonian

$$\hat{H} = \hat{T} + \hat{V}_{QDs} + \hat{V}_M + \hat{r}_{ij}^{-1} + i\hat{W}_z^{L,R} \qquad (1)$$

comprises the typical Cartesian coordinate kinetic energy operators $\hat{T}$ for both electrons and further system-specific potential operators, whose expressions are explained in more detail in the following.

Solid-state QDs are typically embedded in layered structures or in wires and both cases are considered here. The self-assembled or gated QDs fabricated in a lateral arrangement [30, 31, 32, 33] belong to the former class and have a two-dimensional wetting layer into which continuum electrons can be excited and where they become mobile. Only in the QD pair the electrons are confined in all directions. This is modeled by two two-dimensional Gaussians aligned along the z coordinate and centered at x = 0 nm [25] as shown in Fig. 1. In the underlying definition,

$$\hat{V}_{QDs}(x,z) = -D \sum_{j=L,R} \exp\left[-b_j[(\hat{z} - z_j)^2 + \hat{x}^2]\right] \quad (2)$$

j = L, R refers to the left and right QD. The depths D and parameters $b_j = 4\ln(2)/r_j^2$, which determine the potentials' full widths at half maximum $2r_j$, are chosen such that they match experimentally reasonable materials and that there are four levels in the system with $E_{L0} < E_{R0} < E_{L1}^z = E_{L1}^x$ satisfying the ICD energy requirements. The numeric index after L and R counts the levels displayed in Fig. 2. The superscript *x*, *z* refers to the coordinate in which the excitation is polarized.

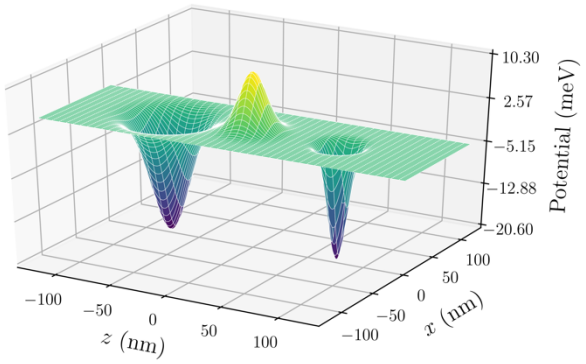

Figure 1. Exemplary potential for two QDs with R = 151.6 nm (15 a.u.) and a barrier in a self-assembled or gated two-dimensional arrangement. The barrier height is DM= 10.3 meV(1.0 a.u.).

The central barrier (Figs. 1 and 2, solid line) or well (Fig. 2, dashed line) placed at the coordinate origin is a third Gaussian,

$$\hat{V}_M = -D_M e^{-b_M[\hat{z}^2 + \hat{x}^2]} \qquad (3)$$

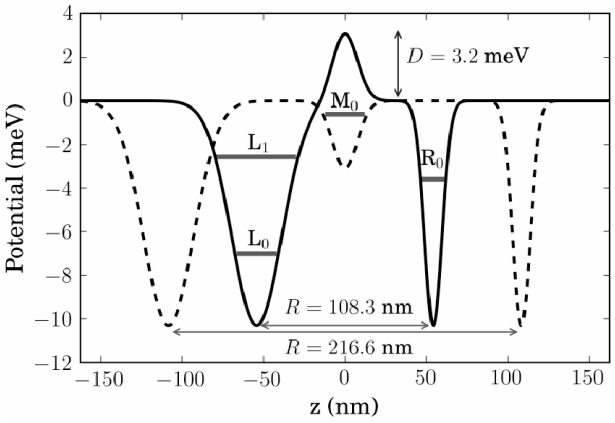

Figure 2. Two exemplary potentials for QDs in a nanowire are shown including an indication for the electronic levels L_0, R_0, M_0, and L_1. The solid line reflects a paired QD with distance of R = 108.3 nm (10 a.u.) among the dot centers and a barrier in the wire of D_M = 3.2 meV (0.311 a.u.) height. The dashed line reflects a QD pair with larger separation of R = 216.6 nm (20 a.u.) with an additional centered well in the wire.

with positive or negative D_M, respectively. In some previous works on QD-ICD such a potential was already used [23, 38]. There was always about as deep as the left or right QD potential and therefore interpreted as a true QD. This makes the main difference to the current work.

In a nanowire [26, 27, 28, 29, 30], the two quantum dots and the central impurity are modeled by Eqs. (2) and (3) both in a one-dimensional formulation neglecting the *x* coordinate. The potential is visualized in Fig. 2. The electron-electron Coulomb interaction $\hat{r}_{ij}^{-1}$ mediating ICD is implemented for the two-dimensional case in its regularized form

$$\hat{r}_{ij}^{-1} \Rightarrow [\hat{r}_{ij}^2 + \alpha^2 . e^{-\beta \hat{r}_{ij}}]^{-1/2} \qquad (4)$$

where the distance among two electrons,

$$r_{12} = |r_1 - r_2| \rightarrow \sqrt{(x_1 - x_2)^2 + (z_1 - z_2)^2}$$

is defined along two Cartesian coordinates only [25]. In the one-dimensional case,

$$\hat{r}_{ij}^{-1} \Rightarrow z_{ij}^{-1} = \sqrt{\frac{\pi}{2l^2}} e^{\zeta^2} (1 - \mathrm{erf}(\zeta)) \quad (5)$$

where $\zeta = |z_1 - z_2|/(\sqrt{2}l)$ and where $l = \sqrt{1/\omega_\perp}$ is an effective length which relates to the width of the nanowire defined through a parabolic confinement with frequency $\omega_\perp$ [39, 40]. Note that we integrate in this way the lateral measures of the nanowire and QDs into the Coulomb interaction potential, which was shown to be a valid approximation for electrons being confined along *x* and *y* when starting from a three-dimensional formulation [39].

For numerical calculations in the MCTDH framework, the potentials (4) and (5) are finally brought into a sum-of-products form, using the multi-grid POTFIT (MGPF) [41] or the standard POTFIT routine [42], respectively.

Also grace to the MCTDH dynamics performed in a finite discrete variable representation (DVR) basis [36, 43, 44], the Hamiltonian (1) accommodates as a last term of the complex absorption potentials (CAPs) [45, 46, 47, 48]

$$i\widehat{W}_c^{L,R} = i\,\eta |c - c^{L,R}|^n \Theta(c - c^{L,R}) \qquad (6)$$

along the relevant coordinates c = *x*, *z* in positive and negative direction. CAPs remove continuous parts of the electronic wave packet from the computation starting at the grid points $c^{L,R}$ as realized by applying a Heavyside function. Further CAP parameters are the strength η and the order *n*.

For the actual dynamics, the initial state is the ICD resonance in which one electron in one QD is excited to one of the differently polarized L_1 states and the other one is bound to the single level R_0 of the other QD. It is prepared in a block improved relaxation calculation. Applying then the equations of motion in real time evolves this initial wave packet until the decay is over. In projecting the time-dependent wave function onto the initial resonance wave function $\Phi^{res}(x, z)$ we obtain the squared autocorrelation function

$$|a(t)|^2 = |\langle \Phi^{res}(x,z) | \Psi(t,x,z) \rangle|^2 = e^{-\frac{\Gamma t}{\hbar}} \quad (7)$$

decaying exponentially and thus allowing to access the decay rate Γ.

3. Computational details

The paper's discussion is based on SI units for GaAs, as those compare well to experimental measures of QDs and to most previous works on QD-ICD. Theoretical findings on other ICD systems, per contra, rely typically on material-independent atomic units, which are more general, so that we

also deliver those. The conversion from atomic to SI units [49] takes the effective mass and the dielectric constant of the moving electron in a GaAs material [50] into account.

As in our previous works, the self-assembled QDs [25] and those in nanowires [51] where parametrized differently and such that they accommodate both the appropriate number of electronic levels in approximately the same range of energies. In the former case, which is depicted in Fig. 1 and defined by Eqs. (2) and (3), the depth of both QDs is identically D = 20.6 meV (2.0 a.u.). This is because their material is the same, namely GaAs, and they are attached to the same external voltage. Note that this is a difference to most of the works in the series on ICD in QDs originating from the first paper in 2011 [9] and also to the work that models a similar three-QD system to what we propose here [23]. The QD widths are $2r_L$ = 36.07 nm (3.33 a.u.) and $2r_R$ = 18.03 nm (1.67 a.u.), which refers to b_L = 0.25 a.u. and b_R = 1.0 a.u., respectively. Thus, the single-electron level energies are E_{L0} = −11.62 meV (−1.128 a.u.) and E_{R0} = −5.43 meV (−0.527 a.u.) for the ground states in the left and the right QD. In the left QD there are further two degenerate x- and *z*-polarized excited states of energy $E_{L1}^{x} = E_{L1}^{z}$= −4.25 meV (−0.413 a.u.).

The impurity has a fixed widths of $2r_M$ = 25.52nm (2.35 a.u., b_M = 0.5 a.u.) while D_M is altered in the range of [−5.15 meV; +10.3 meV] ([−0.5 a.u.; +1.0 a.u.]) in seven uniform steps, such that both barriers and binding sites are represented. Both types of potentials may originate from material boundaries or impurities arising from unwanted or controlled defects [24]. The M_0 state for D_M = −5.15 meV has an energy of E_{M0} = −0.69 meV (0.067 a.u.) and higher energies otherwise, i.e. it remains well above the excited states in the left QD. Thus, it does not affect the energy of any of the other levels. Finally, while the impurity is placed on the coordinate origin, the QDs are centered at $z_{L,R} = \mp 75.81$ nm (7.0 a.u.) with a separation of R = 151.62 nm.

The nanowire QDs (cf. Fig. 2) have likewise both identical confinement depths of D = 10.30 meV (1.0 a.u.). The width parameters $b_{L,R}$ are identical to those of the self-assembled QDs. With that they have the energies E_{L0} = −7.14 meV, E_{L1} = −2.02 meV, and E_{R0} = −3.62 meV (−0.693, −0.196, and −0.351 a.u.). In acknowledgement for the higher computational speed in the one-dimensional computations, the distances among the QD centers are varied within 108.3 nm < R < 324.9 nm (10 - 30 a.u.). Two example settings with R = 108.3 nm (R = 216.6 nm (20 a.u.)) are visualized by solid (dashed) lines in Fig. 2.

The central impurity potential reflects a slice of the nanowire wire of $2r_M$ = 18.03 nm (b_M = 1.0 a.u.) thickness. Further, it has either binding properties (negative D_M up to −5.15 meV (0.5 a.u.), dashed line in Fig. 2) or it has barrier properties (positive D_M up to +10.3 meV (10 a.u.), solid line). For impurity barriers, the number and quality of the levels L_0, R_0, and L_1 remains the same irrespective or the value of D_M. Even the level energy is not changed for the majority of distances R investigated. Just for the shortest distance, the highest energy level L_1 only is slightly pushed up in energy by 4.3 %, where it converges to −1.93 meV (−0.187 a.u.) at D_M = 10.3meV. This is caused by the barrier alternating the upper part of the adjacent QD potentials.

For impurity wells (negative D_M) a single M_0 binding level establishes. It comes in from D_M = −1.5 meV (−0.146 a.u.) and reaches E_{M0}= −1.85 meV (−0.180 a.u.) at the lowest D_M = −5.15 meV for long distances R. If R is comparably small, this energy remains higher due to an avoided crossing with the L_1 level, which in turn is pushed down in energy to −2.4 meV (−0.233 a.u.) at D_M = −5.15 meV. The change in L_1 of course means a change of the transferred energy E and shall alter the rate Γ

monotonically [16, 17]. From the given energies at short distances we can estimate, that the rate at D_M = −5.15 meV shall be 30% smaller than that at D_M = −10.3 meV. At long distance R, no rate change must occur for the energies are constant with D_M variation.

The regularization parameters of the four-dimensional, regularized Coulomb potential of Eq. (4) are α = 0.1 a.u. and β = 100 a.u. [25]. The CAPs (Eq. (6)) are of strength $\eta = 8.7 \cdot 10^{-6}$ and order n = 4. They set on at $c^{L,R}$ = ±866 nm (80 a.u.), while the full DVR grid ends at ±1083.0 nm (100 a.u.). The latter consists of 280 sine points along the *z* and *x* coordinates of both electrons.

4. Results

4.1 One-Dimensional Continuum

The major point of interest in this work is to observe and interpret how a potential centered in the middle of the two QDs affects the dynamics of ICD. Therefore, we prepare the initial two-electron resonance state L_1R_0 in an MCTDH improved relaxation, conduct a propagation, and determine the decay rate. Four rates for different R were plotted in the upper panels of Fig. 3 as function of D_M.

What we see for R = 108.3 nm (10 a.u., left, upper panel) is immensely surprising. The rate of $2.12\text{x}10^{-3}$ meV($2.06\text{x}10^{-4}$ a.u.) at the non-perturbed double QD with D_M = 0 meV turns out to be the global rate maximum. It drops significantly until $0.24\text{x}10^{-3}$ meV ($0.23\text{x}10^{-4}$ a.u) towards negative D_M = −2.7 meV (−0.262 a.u.), which is only 11 % of the original rate. From there it increases only slightly towards the deepest central well considered. It also drops when a barrier is introduced. There the rate reaches values below $1.0 \cdot 10^{-3}$ meV ($0.97\text{x}10^{-4}$ a.u.) from D_M = +2.2 meV (0.214 a.u.) and evolves towards $0.5 \cdot 10^{-3}$ meV.

In disbelieve for this pronounced rate alternation with slight variations of the barrier height or well depth, which hints to a strong impurity effect, we sample further inter-QD distances. Three of them, which increase by 5 a.u. (54.2 nm) each, are explicitly drawn in the three right top panels of Fig. 3. The graph for the doubled distance of R = 216.6 nm (20 a.u., third left, upper panel) closely resembles the previously discussed one. It has a maximum at $2.46\text{x}10^{-5}$ meV ($2.39\text{x}10^{-6}$ a.u.), which drops by one order of magnitude to a minimum of $0.22\text{x}10^{-5}$ meV ($0.21\text{x}10^{-6}$ a.u., 8.7%), when going to lower D_M. The stabilizing value at both, positive and negative D_M is $0.4\text{x}10^{-5}$ meV ($0.39\text{x}10^{-6}$ a.u.). There is, however, a difference. Here, it is the minimal Γ that occurs in the non-perturbed case D_M = 0 meV rather than the maximum before. Moreover, the rates themselves are two orders smaller due to the lowered Coulomb interaction, an effect known from all previous ICD investigations [9, 23].

What seems to be systematic for the rates is disproved with the other two graphs. For R = 162.45 nm (15 a.u., second left, upper panel) the maximal rate of $2.2\text{x}10^{-4}$ meV ($2.14\text{x}10^{-5}$ a.u.) at lowest D_M decreases even by two orders of magnitude to 0.9 % ($0.02\text{x}10^{-4}$ meV, $0.02\text{x}10^{-5}$ a.u.) at D_M = 2.58 meV (−0.250 a.u.) and then continuously increases towards large positive D_M. For R = 270.75 nm (25 a.u., right, upper panel) two maxima occur and the spread between the highest maximum of $1.09\text{x}10^{-5}$ meV($1.06\text{x}10^{-6}$ a.u.) and the lowest minimum of $0.24\text{x}10^{-5}$ meV ($0.23\text{x}10^{-6}$ a.u.) is again in the range of 22%.

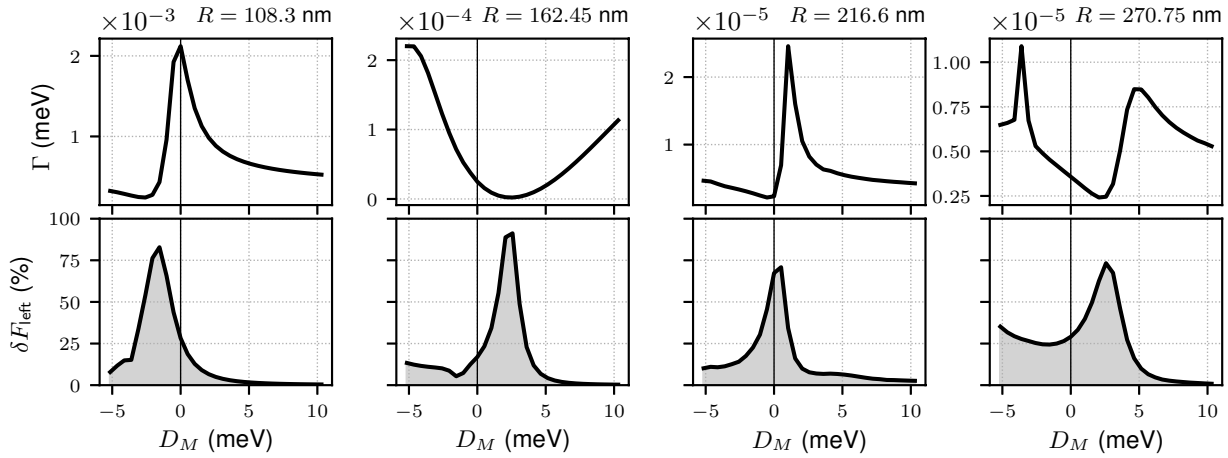

Figure 3: Decay rates Γ in meV (upper panels) and relative fluxes δF_{left} in % of the ICD electron entering the CAP to the left side (lower panels) as function of D_M for four representative distances R increasing from left to right. In a.u. distances are 10, 15, 20, 25. Rates are 10.3 times smaller in a.u.

There is, however, a trend connecting the four panels of Fig. 3. The rates significantly decrease with increasing inter-QD distance. An analytical prediction for such decrease is $\Gamma \propto R^{-6}$ [16, 17] and was proven for many examples of dimer systems, so that ICD rates are often calculated without performing any time propagation [52, 53]. For the particular model of two QDs in a wire, i.e. for a one-dimensional continuum, rates were additionally found to oscillate around the R^{-6} trend in sensitive dependence on the interplay of the Coulomb interaction at the different inter-QD distances as well as the kinetic energy of the continuum electron [9]. Pictorially speaking, the rate depends on if the ICD electron overcomes or tunnels through the double-peaked Coulomb blockade imposed by its bound neighbor electron at the sides of the left QD with energy maximum of about 2.56 meV (0.249 a.u.) for the given QD geometry. If it does, then the ICD electron is found to identical parts on the left and the right side of the paired QD. For cases where the ICD electron has enough energy to overcome the barrier, the rate is the highest. But these cases occurred only when ICD was flawed by electron exchange processes due to the very small distance among the QDs [9]. They are likewise excluded from this study. For tunneling cases the rate was found to have a local minimum due to time losses during the actual tunneling process, whereas rates were large when tunneling is hindered by the double barrier [9].

An interpretation for the extended situation of a simultaneous R and D_M variation of the electronic structure in the given situation of a one-dimensional continuum must necessarily consider the double barrier imposed by the L_0 electron on the ICD electron. It has the same maximum of 2.56 meV throughout. When D_M becomes higher than the energy of the ICD electron of 1.59 meV (0.154 a.u.), then a third maximum arises. Hence, the electron probability on either side of the QD pair with extra well or barrier is determined through the relative flux into the left CAP, δF_{left} [%] = 100 F_{left}/F_{total}. It is displayed for the four exemplary distances in the lower panels of Fig. 3. All graphs support one general and strict connection among Γ and δF_{left}. The maximum of δF_{left} is always paired with the minimum of Γ, which agrees with previous knowledge [9]. There is always one maximum of the relative flux to the left, which illustrates that the complicated barrier structure will allow tunneling to

the left in a limited number of cases.

If D_M is negative, the double barrier created by the L_0 electron around the left binding potential remains unaffected. The ICD electron still experiences the maxima of the Coulomb barrier as its kinetic energy is 1.59 meV and thus below the maximum of the barrier (2.56 meV). More than that, negative D_M lead to a binding well (cf. Fig. 2), whose ionic virtual states can couple to the final ICD states in the superexchange pathway [23]. In cases of setups with other energies and a deeper well than what we have here, it was found to be relevant for R < 195 nm (18 a.u.). As we have here overall shallower wells, the superexchange contribution may already be less important at smaller distances than reported in Ref. [23], i.e. for all but the left-most panels of Fig. 3.

If D_M is positive, then the central potential itself adds a barrier for the ICD electron, which is for most D_M higher than the Coulomb double barrier of about 2.56 meV imposed by the L_0 electron. One further overall trend can be seen from all flux graphs. The relative flux is nearly exclusively to the right side by δF_{left} being below 10% for central barriers above D_M = 5 meV. Note, however, that this does not allow for a clear prediction of the size of the rate.

The inverse condition to the above, namely that at lowest fluxes the rates are highest, does not strictly hold. This can exemplarily be seen from the case of R = 108.3 nm (10 a.u., left panels of Fig. 3). There, at the maximal Γ, δF_{left} = 25% as it is likewise at D_M = −3.2 meV (−0.311 a.u.), where the rate is just slightly larger than its minimal value. Such small rate cases, where barrier tunneling is suppressed, can occur multiple times for one given distance. R = 162.45 nm and R = 270.75 nm (15 and 25 a.u.) do, for instance, lead to two rate maxima.

An overview on the ICD rates as function of both R and D_M is presented in Fig. 4. Marked up as a red, solid-dotted line is the already known oscillating rate-dependence on R for the paired-QD case with D_M = 0 meV. For any fixed value of D_M a comparable trend can be deduced: the rate evolves as $\Gamma \propto R^{-6}$ including oscillations, but the oscillation pattern always differs. If we compare the scenario of two QDs only (red line at D_M = 0) with that for three potentials, or eventually QDs, at the front edge of Fig. 4 (D_M = −5.15 meV), we find a behaviour already observed by Agueny et al. [23]. For similar QDs than ours, but even smaller D_M, the rates nearly perfectly align in their magnitude and oscillation pattern for large R, which the authors explain with the reducing importance of superexchange ICD also valid here. Furthermore, we see a recurrence of the impurity effect already detected from Fig. 3. Upon variation of D_M there are two pronounced lines of maximal rates along two diagonals of Fig. 4 evolving each from a combination of smaller R and D_M towards simultaneously increased values of the two. Considering the previous discussion, the rate maxima arise from a complex interplay of the energetic conditions of the system-based Coulomb barriers and kinetic energies.

To wrap up, this impurity effect of quick and strong ICD rate alternations by up to two orders of magnitude is experienced in QDs embedded in nanowires when an electrical or material impurity is introduced in their middle on the nanowire and likewise when their inter-QD distance is changed leading both to changes of the electronic structure and with that the dynamics. The impurity effect is significant due to the confinement of electronic motion along the dimension in which the Coulomb interaction is effective. We explain that it is caused

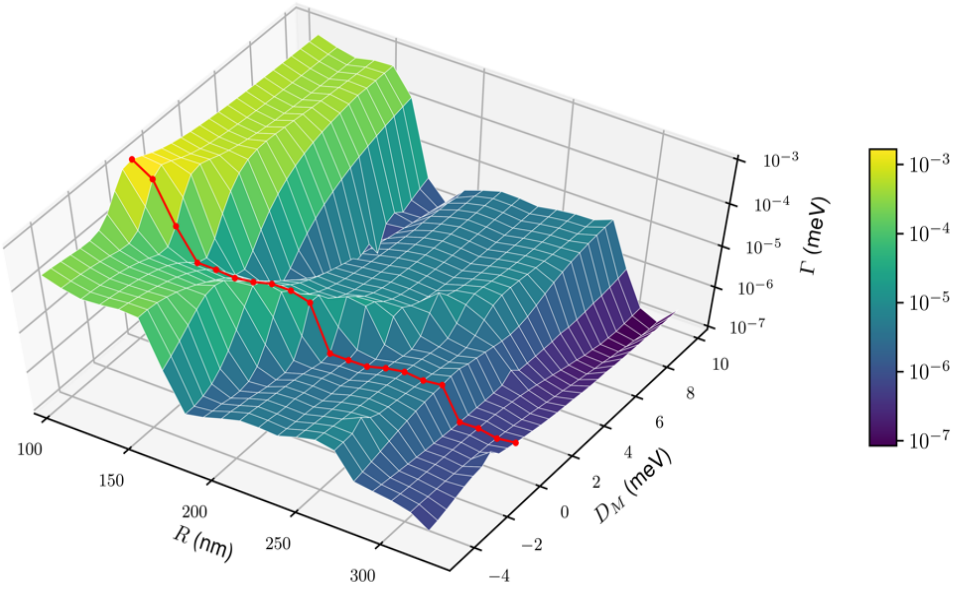

Figure 4: Dependence of decay rates Γ in logarithmic representation on the distance R of the QDs and the orientation and size of the impurity in the nanowire captured in central potential prefactor D_M . The red line marks the unperturbed case of two QDs only. Decay rates Γ as function of D_M for R = 151.6 nm (15 a.u.) in QDs with a two-dimensional continuum.

by the Coulomb barrier imposed on the ICD electron, so we assume it to significantly reduce for QDs with a lower degree of confinement for the ICD electron.

4.2 Two-Dimensional Continuum

Of course, most of the known ICD systems are of atomic or molecular nature and therefore are not limited in the emission direction of the ICD electron with having a three-dimensional continuum. Indeed, in such systems there are also no oscillations in the R^{-6} rate decrease. Furthermore, with a central spherical binding potential, the rate also monotonically follows changes in R [20, 21]. An intermediate case previously investigated with electron dynamics are laterally-arranged self-assembled [31, 32, 33], as well as gated 2DEG [30] QDs with a two-dimensional ionization continuum in their wetting layer [25]. There, rate fluctuations upon R-variation around the R^{-6} least squares fit to Γ got significantly reduced from a maximum (average) of 222% (85%) in the case of a one-dimensional continuum to 50% (24%) for the decay of the resonance with excitation along z [25]. It is meaningful to also check the relevance of the impurity effect observed for D_M variation for an increasing number of continuum dimension along the same lines.

To this end we reset the Hamiltonian using expressions (2) and (3), adjust the parametrization (R = 151.6 nm, 14 a.u.) to the boundary conditions, create an initial state that is either *x* or *z* polarized, propagate and evaluate the rates from the decaying autocorrelation function. The results are shown in Fig. 5. As the energy levels accommodated in this two-dimensional potential have changed with its shape, and the distance R has increased compared to the previous standard case, the rates are now of the order of 10^{-5} meV.

The solid line in the graph represents the decay of the z-excited resonance state that is the counterpart to the ICD in a one-dimensional system. Γ has a maximum of 0.94×10^{-5} meV (3.83×10^{-6} a.u.) at negative D_M = −2.58 meV (−0.250 a.u.).

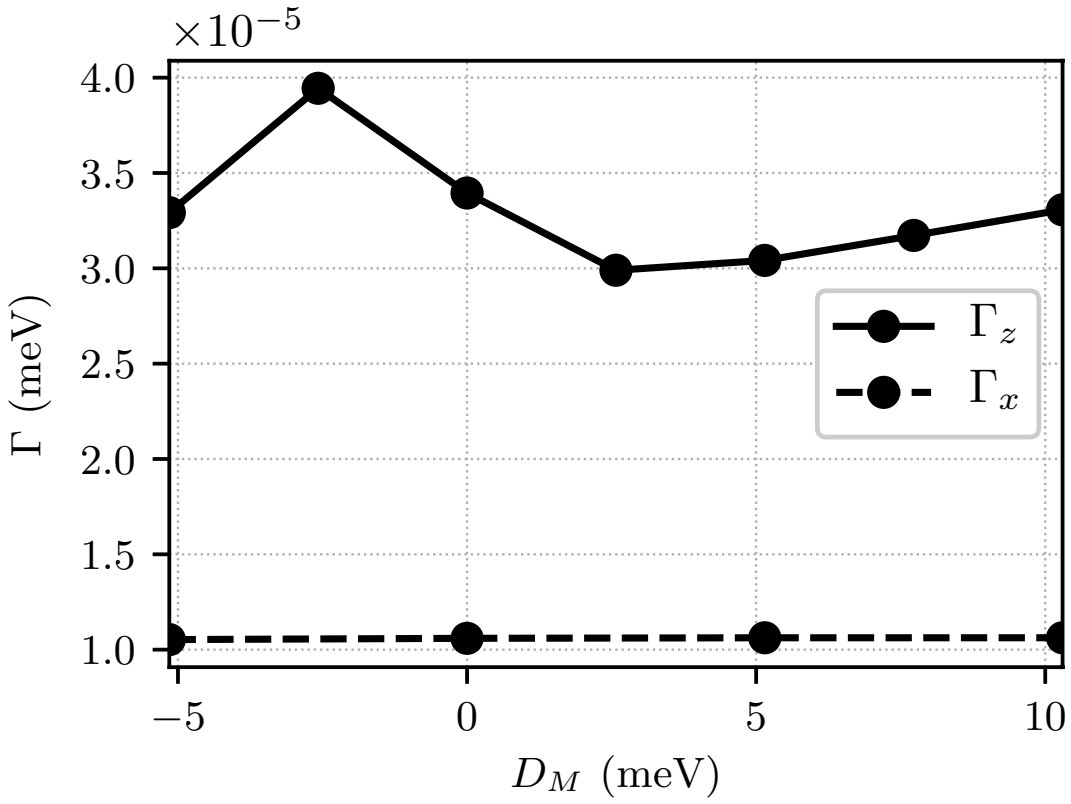

Figure 5: Decay rates Γ as function of D_M for R = 151.6 nm (15 a.u.) in QDs with a two-dimensional continuum

Towards smaller D_M the rate decreases until $3.29 \times 10^{-5}\ meV (3.19 \times 10^{-6})\ a.u.$ at negative D_M = −5.15 meV, however, without passing a local minimum. The global minimum occurs at D_M = 2.58 meV which displays a rate $\Gamma = 2.99 \times 10^{-5}\ meV (2.90 \times 10^{-6}\ a.u)$ before it resumes to $3.31 \times 10^{-5}\ meV\ (3.21 \times 10^{-6}\ a.u.)$ The graph has an intermediate behavior between those for R = 108.3 nm and for R = 162.45 nm (10 and 15 a.u.) in the one-dimensional case. The impurity effect is much less pronounced, because the difference between rate minimum and maximum is only about 25% compared to above 99 % before. This meets the expectation that the ICD electron may circumvent the Coulomb barrier by spreading onto the *x* − *z* plane and is therefore less affected by effects of only one dimension [25]. The result suggests therefore that the more dimensions are available to the ICD electron the smaller is the impurity effect.

The ICD of the x-polarized resonance electron with emission of the R_0 electron along the x direction supports this statement. The respective graph is shown as a dashed line in Fig. 5). It reveals that the rate Γ_x is totally independent of D_M .

5. Discussion

What would the overall findings mean for the ICD process in general and for a device application in particular? In all the atomistic and molecular examples two limitations influential to the impurity effect are lifted. On the one hand, there are energetic limitations. The central disturbance in a molecular framework would be another atom or molecule and hence be necessarily electron binding (i.e. $D_M < 0$ meV). This has been investigated in the context of superexchange ICD [20, 21, 23]. There, the atom or QD is placed in the middle of the original ICD participators and accelerates ICD in that it offers an additional ICD pathway at short distances through perturbative coupling among virtual states of a central anion site and the final states [20]. The pronounced difference to what is studied here is that for superexchange ICD the distance from the emitter to the central potential must be small to allow for a coupling of the final ionized state with the anionic (charge-transfer or tunneling) virtual states. This was just recently confirmed with an analytic rate equation including the superexchange term [20, 23]. Here we encounter many cases with large distances ($R > 150$ nm) of which we know that tunneling is forbidden [9]. There, also superexchange cannot be relevant, while we observe the impurity effect. And especially also impurities leading to an energy barrier, to remain important.

On the other hand there are limitations regarding the electron emission direction. In atoms and molecules it is fully free, i.e. the electron can escape in all spatial dimensions, whereas in QDs it may be restricted to two or even one dimension. When considering the fact that in the quantum dot examples of this paper the maximal rate variation with changing perturbation through D_M decreases from above 99% (1D) to about 25 % (2D), then we must assume a significantly smaller effect in three dimensions. This is supported by comparing $\Gamma - R$ curves for cases with different dimensionality of the ionization continuum [9, 25, 17], which show that rates follow R^{-6} more strongly the more spatial freedom there is for the ICD electron. These two aspects lead to the conclusion that the impurity effect in ICD is majorly of importance in strongly confined systems where the emission direction is driven through the environment near the emitter, i.e. a gate voltage or an embedding in a confined wire structure. Note that in an experiment like COLTRIMS [54, 55] in which electrons are directed towards a detector by strong anisotropic magnetic fields, no impurity effect is expected, because the field only applies at a significant distance from the atomic cluster in which ICD occurs.

To wrap up, among the known ICD system, quantum dots embedded in a nanowire and quantum dots with gating to confine electronic motion in one dimension only, are the ones that shall experience the strongest effect for the ICD rate when an electrical or material impurity is introduced in their middle on the wire. This is tightly followed by laterally-arranged self-assembled QDs. In this realm of nanostructures and with view on a technical realization of ICD in QDs, the impurity effect is curse and blessing at the same time.

On one side of the medal, it suggests that small inaccuracies in the fabrication or electric gating of nanowire QDs will lead to impurities in the widest sense and to a significantly randomized rate. With that it may be difficult to experimentally prove a theoretically predicted ICD rate beyond the order of magnitude. If integrated in a device, its reproducible fabrication may suffer from the effect

as well. Only recently it was possible to grow defect-free nanowires with QDs so this drawback may be overcome in the near future [56].

The other side of the medal is that random quality fabricates may a posteriori be adjusted to the desired rate by imposing gates. There is a chance that with careful tuning by gate voltages, ICD could be made faster and thus more competitive with adverse processes even for longer distances R. We have here the phonon-mediated decay in mind, which was recently discussed in detail for the QDs in the nanowire with a geometry leading to an ICD rate of 10^{-3} meV [51]. It was found to be at least one order of magnitude slower than ICD. At the intermediate distances 162.45 nm and 216.6 nm, which are longer than the distances studied earlier 86.7 nm [9], ICD may still be competitive to phonon-mediated decay for those D_M where the rate Γ is largest.

If the device was to detect and enhance the current of the ICD electron rather than the rate, a chance lies in optimizing such current through the electron flux by significantly increasing the central barrier and direct the ICD electron away from the excited QD.

6. Conclusions

This study on the interparticle Coulombic decay in pairs of electron binding potentials with spatially confined continuum brought forth how strongly the ICD electron emission and the overall rate depend on the presence and slightest modification of a centrally-located binding site or repulsive barrier, i.e. an impurity. The impurity effect is the strongest geometry-induced ICD rate enhancement reported to present. It is furthermore more pronounced the stronger the ICD electron is confined. Therefore its significance in solid-state nanowires based on quantum dot arrays is higher than in atomic/molecular clusters. In such devices it can be induced by material, geometric, or electrostatic modifications within the nanostructure and be used to control QD-ICD.

Acknowledgments

The project was financially supported by the Volkswagen Foundation through the Freigeist Fellowship No. 89525 and by the Summer Student Program of the Helmholtz-Zentrum Berlin. We thank the Helmholtz-Zentrum Dresden-Rossendorf for granting us access to their GPU server.

References and Notes

[1] CEDERBAUM, L. S.; ZOBELEY, J.; TARANTELLI, F. Giant intermolecular decay and fragmentation of clusters. Phys. Rev. Lett., v. 79, p. 4778, 1997.

[2] FANO, U. Effects of configuration interaction on intensities and phase shifts. Phys. Rev., v. 124, p. 1866, 1961.

[3] FESHBACH, H. Unified theory of nuclear reactions. Ann. Phys., v. 5, p. 357, 1958.

[4] FESHBACH, H. A unified theory of nuclear reactions. ii. Ann. Phys., v. 19, p. 287, 1962.

[5] SANTRA, R.; ZOBELEY, J.; CEDERBAUM, L. S. Electronic decay of valence holes in clusters and condensed matter. Phys. Rev. B, v. 64, p. 245104, 2001.

[6] ZOBELEY, J.; SANTRA, R.; CEDERBAUM, L.S. Electronic decay in weakly bound heteroclusters: Energy transfer versus electron transfer. J. Chem. Phys., v. 115, p. 5076, 2001.

[7] MORISHITA, Y. et al. Experimental evidence of interatomic Coulombic decay from the auger final states in Argon dimers. Phys. Rev. Lett., v. 96, p. 243402, 2006.

[8] SISOURAT, N. et al. Ultralong-range energy transfer by interatomic Coulombic decay in

an extreme quantum system. Nature Phys., v. 6, p. 508–511, 2010.

[9] BANDE, A.; GOKHBERG, K.; CEDERBAUM, L. S. Dynamics of interatomic Coulombic decay in quantum dots. J. Chem. Phys., v. 135, p. 144112, 2011.

[10] CHERKES, I.; MOISEYEV, N. Electron relaxation in quantum dots by the interatomic Coulombic decay mechanism. Phys. Rev. B, v. 83, p. 113303, 2011.

[11] GOLDZAK, T. et al. Interatomic coulombic decay in two coupled quantum wells. Phys. Rev. B, v. 91, p. 165312, 2015.

[12] AVERBUKH, V.; CEDERBAUM, L. S. Interatomic electronic decay in endohedral fullerenes. Phys. Rev. Lett., v. 96, p. 053401, 2006.

[13] DE, R. et al. First prediction of inter-Coulombic decay of C_{60} inner vacancies through the continuum of confined atoms. J. Phys. B, v. 49, p. 11LT01, 2016.

[14] UNGER, I. et al. Control of X-ray induced electron and nuclear dynamics in ammonia and Glycine aqueous solution via hydrogen bonding, J. Phys. Chem. B, American Chemical Society, v. 119, p. 10750, 2015.

[15] WILHELM, R. A. et al. Interatomic Coulombic decay: The mechanism for rapid deexcitation of hollow atoms. Phys. Rev. Lett., v. 119, p. 103401, 2017.

[16] SANTRA, R.; CEDERBAUM, L. S. Non-Hermitian electronic theory and applications to clusters. Phys. Rep., v. 368, p. 1, 2002.

[17] AVERBUKH, V.; MÜLLER, I. B.; CEDERBAUM, L. S. Mechanism of interatomic coulombic decay in clusters. Phys. Rev. Lett., v. 93, p. 263002, 2004.

[18] DOLBUNDALCHOK, P. et al. Geometrical control of the interatomic Coulombic decay process in quantum dots for infrared photodetectors. J. Comput. Chem., v.37 p.2249, 2016.

[19] WEBER, F.; AZIZ, E. F.; BANDE, A. Interdependence of ICD rates in paired quantum dots on geometry. J. Comput. Chem., v. 38, p. 2141, 2017.

[20] MITEVA, T. et al. Interatomic Coulombic decay mediated by ultrafast superexchange energy transfer. Phys. Rev. Lett., v. 119, p. 083403, 2017.

[21] VOTAVOVÁ, P. et al. Mechanism of superexchange interatomic Coulombic decay in rare-gas clusters. Phys. Rev. A, v. 100, p. 022706, 2019.

[22] BENNETT, R. et al. Virtual photon approximation for three-body interatomic Coulombic decay. Phys. Rev. Lett., v. 122, p. 153401, 2019.

[23] AGUENY, H. et al. Interparticle Coulombic decay in coupled quantum dots: Enhanced energy transfer via bridge assisted mechanisms. Phys. Rev. B, v. 101, p. 195431, 2020.

[24] SCHROER, M. D.; PETTA, J. R. Correlating the nanostructure and electronic properties of InAs nanowires. Nano Lett., v. 10, p. 1618, 2010.

[25] HALLER, A.; PELÁEZ, D.; BANDE, A. Inter-Coulombic decay in laterally arranged quantum dots controlled by polarized lasers. J. Phys. Chem. C, v. 123, p.14754–14765, 2019.

[26] LETURCQ, R. et al., Franck-Condon blockade in suspended carbon nanotube quantum dots, Nature Phys., v. 5, p. 327, 2009.

[27] SALFI, J. et al. Electronic properties of quantum dot systems realized in semi-conductor nanowires. Semicond. Sci. Technol., v. 25, p. 024007, 2010.

[28] RODDARO, S. et al. Manipulation of electron orbitals in hard-wall InAs/InP nanowire quantum dots. Nano Lett., v. 11, p. 1695, 2011.

[29] Nadj-Perge, S. et al. Spectroscopy of spin-orbit quantum bits in indium antimonide nanowires. Phys. Rev. Lett., v. 108, p. 166801, 2012.

[30] van der Wiel, W. G. et al. Electron transport through double quantum dots. Rev. Mod. Phys., v. 75, p. 1, 2002.

[31] PETROFF, P. M.; LORKE, A.; IMAMOGLU, A. Phys. Today, v. 52, p. 46, 2001.[32] WANG, L. et al. Self-assembled quantum dot molecules. Adv. Mater., v. 21, p. 2601, 2009.

[33] ZALLO, E. et al. Epitaxial growth of lateral quantum dot molecules. Phys. Stat. Sol. B, v. 249, p. 702, 2012.

[34] MEYER, H.-D.; MANTHE, U.; CEDERBAUM, L. The multi-configurational time-dependent Hartree approach. Chem. Phys. Lett., v. 165, p. 73 , 1990.

[35] MANTHE, U.; MEYER, H.; CEDERBAUM, L. S. Wave-packet dynamics within the multiconfiguration Hartree framework: General aspects and application to NOCl. The Journal of Chemical Physics, v. 97, p.

3199–3213, 1992.

[36] BECK, M. et al. The multiconfiguration time-dependent Hartree (MCTDH) method: a highly efficient algorithm for propagating wavepackets. Phys. Rep., v. 324, p. 1, 2000.

[37] MEYER, H.-D.; GATTI, F.; WORTH, G. A. (Ed.). Multidimensional quantum dynamics: MCTDH theory and applications. Weinheim: Wiley-VCH, 2009.

[38] LANGKABEL, F.; LÜTZNER, M.; BANDE, A. Interparticle Coulombic decay dynamics along single- and double-ionization pathways. J. Phys. Chem. C, v. 123, p. 21757, 2019.

[39] BANDE, A. et al. Dynamics of interatomic Coulombic decay in quantum dots: Singlet initial state. EPJ Web Conf., v. 41, p. 04031, 2013.

[40] BEDNAREK, S. et al. Effective interaction for charge carriers confined in quasi-one-dimensional nanostructures. Phys. Rev. B, v. 68, p. 045328, 2003.

[41] PELÁEZ, D.; MEYER, H.-D. The multigrid potfit (mgpf) method. Grid representations of potentials for quantum dynamics or large systems. J. Chem. Phys., v. 138, p. 014108, 2013.

[42] JÄCKLE, A.; MEYER, H.-D. Product representation of potential energy surfaces. J. Chem. Phys., v. 104, p. 7974, 1996.

[43] LIGHT, J. C. Time-dependent quantum molecular dynamics. In: Plenum: New York, 1992. p. 185.

[44] LIGHT, J. C.; Carrington Jr, T., Discrete variable representations and their Utilization, Adv. Chem. Phys., v. 114, p. 263, 2000.

[45] NEUHAUSER, D.; BAER, M., A three-dimensional quantum mechanial study of vibrationally resolved charge trandfer processes in $H^+ + H_2$ at E_{cm}=20 eV, J. Chem. Phys., v. 90, p. 4351, 1989.

[46] NEUHAUSER, D.; BAER, M.; Judon, R. S. and Kouri, D. J., The application of time-dependent wavepacket methods to reactive scattering, Comput. Phys. Comun., v. 63, p. 460, 1991.

[47] RISS, U. V.; MEYER, H.-D., Calculation of resonance energies and widths using the complex absorbing potential method, J. Phys. B, v. 26, p. 4503, 1993.

[48] RISS, U. V.; MEYER, H.-D. Investigation on the reflection and transmission properties of complex absorbing potentials. J. Chem. Phys., v. 105, p. 1409, 1996.

[49] BANDE, A. Electron dynamics of interatomic Coulombic decay in quantum dots induced by a laser field. J. Chem. Phys., v. 138, p. 214104, 2013.

[50] NSM Archive Physical Properties of Semiconductors.http://matprop.ru/GaAs_basic, accessed on November 21, 2018.

[51] BANDE, A. Acoustic phonon impact on the inter-Coulombic decay process in charged quantum dot pairs. Mol. Phys., v. 117, n. 15-16, p. 2014, 2019.

[52] AVERBUKH, V. et al. Quantum Chemical Approach to Interatomic Decay Rates in Clusters, Netherlands: Springer, 2009. In: Advances in the Theory of Atomic and Molecular Systems, v. 20, p. 155.

[53] KREIDI, K. et al. Photo- and Auger-Electron Recoil Induced Dynamics of Interatomic Coulombic Decay. Phys. Rev. Lett., v. 103, n. 3, p. 033001, 2009.

[54] KRUIT, P.; READ, F. H. Magnetic field paralleliser for 2pi electron-spectrometer and electron image magnifier. J. Phys. E: Sci. Instrum., v. 16, p. 313, 1983.

[55] MUCKE, M. et al. A hitherto unrecognized source of low-energy electrons in water. Nat. Phys., v. 6, p. 143, 2010.

[56] WU, J. et al. Defect-free self-catalyzed GaAs/GaAsP nanowire quantum dots grown on silicon substrate. Nano Lett., v. 16, p. 504, 2016.